Online supplement

The Fms-like tyrosine kinase-3 ligand/lung dendritic cell axis contributes to regulation of pulmonary fibrosis

Meritxell Tort Tarrés, Franziska Aschenbrenner, Regina Maus, Jennifer Stolper, Lisanne Schütte, Lars Knudsen, Elena Lopez Rodriguez, Danny Jonigk, Mark Kühnel, David S. DeLuca, Antje Prasse, Tobias Welte, Jack Gauldie, Martin Kolb and Ulrich A. Maus

Methods

Mice

WT mice (C57BL/6N and C57BL/6J) were purchased from Charles River (Sulzfeld, Germany). Flt3L KO mice on a C57BL/6N background (1) and their respective control mice were purchased from Taconic (Germantown, New York). Batf3 (Basic leucine zipper transcription factor, ATF-like 3) KO mice, CD45.1 alloantigen expressing C57BL/6J WT mice (B6.SJL-Ptprca), and CD103 KO mice, all on a C57BL/6J background, were purchased from The Jackson Laboratory (Bar Harbor, Maine). $zDC^{+/DTR}$ mice bearing the human diphtheria toxin receptor under control of the classical DC-specific zinc finger transcription factor zDC (also termed Zbtb46 and Btbd4) were generously provided by Michel Nussenzweig (The Rockefeller University, New York) (2). Animals were kept under individually ventilated cage (IVC) conditions with free access to food and water, unless otherwise stated, and were used for experiments at 8 to 12 weeks of age.

Reagents

Antibodies employed for flow cytometric analysis including anti-CD11b PE-Cy7 (clone M1/70, rat IgG_{2a}), anti-CD103 BV 510 (clone M290, rat IgG_{2a}) and anti-MHC class II PE (clone M5/114, rat IgG_{2b}) were obtained from BD Biosciences (Heidelberg, Germany). Anti-CD11c eFluor 450 (clone N418, armenian hamster IgG) was obtained from eBioscience (San Diego, CA). For immunofluorescence, we used purified rat anti-mouse I-A/I-E (MHCII, Biolegend, clone M5/114.15.2) in conjunction with AlexaFluor 568 conjugated secondary goat anti-rat antibody (ThermoFisher), and anti-mouse CD11c AlexaFluor 647 (Biolegend, clone N418), as well as purified mouse anti-human HLA-DR (Biolegend, clone L243) in conjunction with AlexaFluor 568 conjugated secondary rat anti-mouse IgG (ThermoFisher), and anti-human

Tort Tarrés M, *et al. Thorax* 2019; 0:947–957. doi: 10.1136/thoraxjnl-2018-212603

CD11c AlexaFluor 647 (Biolegend, clone 3.9). Diphtheria toxin was purchased from Merck (Darmstadt, Germany). Clinical grade recombinant human Flt3L (CDX-301) was generously provided by Celldex Therapeutics (Hampton, New Jersey).

Adenoviral gene transfer of biologically active TGF-β1

Replication-deficient adenoviral vectors without gene insertion (empty control vector, Ad CL), or vector containing the biologically active form of the porcine TGF-β1 gene (AdTGF-$\beta1^{223/225}$) were prepared as previously detailed (3). WT mice, or Flt3L KO mice, or CD103 KO mice, or Batf3 KO mice, or in selected experiments, chimeric $zDC^{+/DTR}$ mice were anesthetized with an intraperitoneal injection of xylazine (3 mg/kg body weight; Bayer, Leverkusen, Germany) and ketamine (75 mg/kg; Albrecht, Aulendorf, Germany), and were then subjected to intratracheal aspiration of 10^8 plaque-forming units of respective AdTGF-β1 or empty control (AdCL) vectors, as recently described (4).

Bronchoalveolar lavage and quantification of leukocyte subsets

Mice were euthanized with an overdose of isoflurane (AbbVie, Ludwigshafen, Germany) and tracheas were cannulated with a shortened 20-gauge needle. Bronchoalveolar lavage (BAL) was performed as previously described in detail (5).

Determination of collagen contents

Lung collagen contents were determined by hydroxyproline dye binding assay according to published protocols (4).

Immunophenotypic analysis of pulmonary dendritic cells and macrophages

Tort Tarrés M, *et al. Thorax* 2019; 0:947–957. doi: 10.1136/thoraxjnl-2018-212603

Flow cytometric immunophenotypic analysis of lung dendritic cells and macrophages was performed as recently described (6). Briefly, lungs of mice were perfused with HBSS, dissected into small pieces and digested in RPMI/collagenase A (5 mg/ml) and DNase I (1 mg/ml) (Roche, IN) at 37°C for 90 min. Afterwards, single cell suspensions were obtained by filtration, and CD11c-positive lung leukocyte subsets were enriched by magnetic cell purification (Miltenyi, Bergisch Gladbach, Germany). After pre-incubation with Octagam (Octapharma, Langenfeld, Germany), cells were stained with fluorochrome-conjugated monoclonal antibodies with specificity for CD11b, CD11c, CD103, and MHC II for 20 min at 4°C. Subsequently, cells were washed with FACS buffer and subjected to FACS analysis of respective DC subsets. Classical lung DC subsets were gated according to their forward scatter area (FSC-A) versus side scatter area (SSC-A) characteristics and their low green autofluorescence properties, in conjunction with their $CD11c^{pos}$, $MHCII^{pos}$, $CD11b^{hi}$, $CD103^{neg}$ ($CD11b^{pos}$ DC) or $CD11c^{pos}$, $MHCII^{pos}$, $CD11b^{low}$, and $CD103^{pos}$ ($CD103^{pos}$ DC) antigen expression profiles. Data acquisition was performed on a BD FACSAria III flow cytometer (BD Biosciences, Heidelberg, Germany) equipped with a 4-laser system and a 85-µm ceramic nozzle. Data analysis and fluorescence compensation of spectral overlaps was performed using BD FACSDiva Software. Total cell numbers of respective leukocyte subsets were calculated by multiplication of percent values of the respective leukocyte subset obtained by FACS analysis with total cell counts of purified $CD11c^{pos}$ cells.

Fluorescence-activated cell sorting of pulmonary dendritic cells

Lung $CD11b^{pos}$ and $CD103^{pos}$ DC were subjected to fluorescence-activated cell sorting for subsequent next generation sequencing analysis, as described below, as well as analysis of defined markers of extracellular matrix (ECM) turnover and matrix

Tort Tarrés M, *et al. Thorax* 2019; 0:947–957. doi: 10.1136/thoraxjnl-2018-212603

metalloproteases (MMPs) by real-time RT-PCR (see below). Briefly, lung DC subsets were gated as outlined above, and flow sorting was performed using a BD FACSAria III flow cytometer (BD Biosciences, Heidelberg, Germany) equipped with a 85-µm ceramic nozzle. All cell sorts were performed at a constant temperature of 4º C at a flow rate of 3,000 particles per second to ensure high sort efficiency. Post-sort analysis of sorted DC subsets confirmed sort purities of > 95 %.

Determination of Flt3L levels in mice and patients with interstitial lung fibrosis

For quantification of serum Ftl3L protein levels in mice, blood was collected from the Vena cava into microtubes (Sarstedt, Nümbrecht, Germany). Human serum was sampled during routine laboratory diagnostics of ILD patients or disease controls. Subsequently, samples were incubated for 30 min at room temperature, and after centrifugation (3500 rpm, 15 min, RT), sera were carefully collected and Flt3L protein was measured by enzyme-linked immunosorbent assay (R&D Systems, Minneapolis, MN) following the manufacturer's instructions (detection limit 31 pg/ml).

Human explant lung tissue specimen were retrieved from the biobank of Hannover Medical School and were collected either from peripheral lung tissue of patients with end-stage lung fibrosis (n=18, details see supplement), or from disease-free peripheral lung tissue of patients with lung carcinoma serving as disease controls (n=10) by an experienced lung pathologist (DJ). Lung tissue pieces were weighed and homogenized in PBS supplemented with protease inhibitor cocktail (Merck, Darmstadt, Germany) to provide a final concentration of 500 mg tissue/ml PBS. Samples were then homogenized and centrifuged at 13,000 rpm at 4°C for 10 minutes. Lung tissue homogenate supernatants were then aspirated and again subjected to centrifugation to eliminate subcellular constituents from further analysis.

Tort Tarrés M, *et al. Thorax* 2019; 0:947–957. doi: 10.1136/thoraxjnl-2018-212603

Subsequently, human Flt3L protein was measured using commercially available ELISA (R&D Systems).

Immunofluorescence analysis

Lungs of mice were instilled with 600 µl of a mixture of 4 % paraformaldehyde (PFA) and 8 % saccharose, and were then removed and washed two times in PBS. Human lung tissue specimen was collected by an experienced pathologist during routine inspection and subsequent histopathological examination of lung explants. After incubation for 15 minutes in 4 % PFA for fixation at room temperature, lung lobes were dissected from bronchial trees and were transferred for 2 h each in 5 ml 10 %, and 20 % saccharose solution, and were then kept in 30 % saccharose solution overnight at 4 °C. Freezing of lung lobes was done in cryomold wells filled with O.C.T. Tissue Tek (Fa. Sakura) in liquid-nitrogen, and were then stored at -80°C. Sectioning of frozen lung tissue was performed with a cryostat (Leica CM1900 UV) at -25°C at 4 µm, and sections were then mounted on Superfrost Plus slides (Thermo Fisher). Lung sections were encircled with PAP-Pen (Fa. Sigma Aldrich) and fixed with 4 % PFA for 15 minutes, and were then washed two times for 3 min with PBS + 0,05 % TWEEN. Blocking of sections was done with PBS/5 % FCS for 30 min in humidity chambers at room temperature. For staining of human lung tissue, sections were incubated with mouse anti-human I-A/I-E (MHCII, dilution 1:400), and secondary rat anti-mouse AF568, after which sections were washed and stained with anti-mouse CD11c-AlexaFluor 647 (dilution 1:200). Mouse lung tissue sections were stained with rat anti-mouse MHCII, followed by secondary AF568-conjugated goat anti-rat Ab. Subsequently, sections were washed and stained with rat anti-mouse CD11c-AF647. Incubation of antibody cocktails was done for 1 h in humidity chambers at room temperature in the dark followed by three washing steps with PBS

Tort Tarrés M, *et al. Thorax* 2019; 0:947–957. doi: 10.1136/thoraxjnl-2018-212603

+ 0,05 % TWEEN. Slides were rinsed with distilled water and overlaid with mounting medium containing nuclear DAPI stain (Roti Mount Fluor Care, Carl Roth) and cover slips. Examination of lung tissue sections was done with a Zeiss Axio Observer 7 inverted fluorescence microscope equipped with a Colibri LED light source, a plan-apochromatic 20 x lens, a Zeiss apotome 2 for optical sectioning, and a high dynamic range camera (Zeiss, model FK-506). Analysis of fluorescence images was done on a Zeiss Zen2 Pro software platform.

Lung histopathology

Histopathological examination of lung tissue sections of WT mice versus Flt3L KO mice exposed to adenoviral vectors for 14 days was performed as recently described (19). Briefly, paraffin-embedded lung sections (2.5 µm) were prepared as detailed above, and were then stained with hematoxylin/eosin (HE) and trichrome (Elastica-van-Gieson). Subsequently, histopathological examination was performed by an experienced lung pathologist (DJ) blinded to respective treatment condition. Representative photographs were taken at the indicated magnifications using a Zeiss Axiovert 200 M microscope (Carl Zeiss, Oberkochen, Germany).

Generation of chimeric zDC$^{+/DTR}$ mice

In selected experiments, we employed chimeric zDC$^{+/DTR}$ mice allowing selective diphtheria toxin-induced depletion of DC while sparing macrophages (2) to examine the effect of DC depletion on lung fibrosis and lung mechanics in AdTGFβ1-exposed mice. Briefly, CD45.1 alloantigen expressing donor C57BL/6J mice were subjected to whole body irradiation (6 Gy) followed by i.v. injection of purified bone marrow cells (10^7 cells/mouse) collected from CD45.2^{pos} zDC$^{+/DTR}$ mice. Bone marrow transplanted

Tort Tarrés M, *et al. Thorax* 2019; 0:947–957. doi: 10.1136/thoraxjnl-2018-212603

mice were kept in individually ventilated cage (IVC) conditions with access to autoclaved food and water until full reconstitution of their hematopoietic system for 7 weeks, and only mice with >92 % hematopoietic engraftment of CD45.2^{pos} leukocytes were used for experiments.

Diphtheria toxin dependent depletion of cDC

Diphtheria toxin was administered intraperitoneally in WT chimeric mice (serving as controls) and in zDC$^{+/DTR}$ bone marrow chimeric mice to deplete classical dendritic cells (cDC), based on published reports (2). WT bone marrow chimeric mice (WT CD45.2 onto WT CD45.1, transplantation controls) and zDC$^{+/DTR}$ bone marrow chimeric mice initially received 20 ng DT/g body weight (b.w.), followed by 10 ng DT/g b.w. on day 3 after the initial DT injection, and every third day thereafter for up to 14 days.

Assessment of respiratory mechanics

WT mice and Flt3L KO mice as well as WT and zDC$^{+/DTR}$ chimeric mice exposed to adenoviral vector were subjected to pulmonary function tests using a FlexiVent FX (SCIREQ, Montreal, Quebec, Canada) small animal ventilator, as recently outlined in detail (7). Briefly, mice were anesthetized with an intraperitoneal (i.p.) injection of xylazine (3 mg/kg body weight; Bayer, Leverkusen, Germany) and ketamine (75 mg/kg; Albrecht, Aulendorf, Germany), and after relief of pain reflexes a catheter was surgically inserted and fixed into the trachea. Subsequently, animals were connected to baseline mechanical ventilation (10 ml/kg body weight, 150 ventilations/min, positive end-expiratory pressure (PEEP) 3 cm H_2O, and inspiratory-to-expiratory ratio 1:2), and were then additionally i.p. injected with xylazine, ketamine and pancuronium (0.8 mg/kg; Actavis, Munich, Germany). After few minutes, steady state conditions

Tort Tarrés M, *et al. Thorax* 2019; 0:947–957. doi: 10.1136/thoraxjnl-2018-212603

were documented by stable tissue elastance and resistance data, so that a derecruitability test (PEEP 3 cm H_2O) was performed consisting of two recruitment maneuvers, followed by baseline ventilation and lung mechanics assessment at 30-s intervals using the forced oscillation technique (FOT). Tissue elastance (H) reflecting lung stiffness was calculated by fitting the constant-phase model to FOT-derived impedance spectra as previously described (8). Subsequently, two recruitment maneuvers and three pressure-controlled quasi-static pressure-volume (PV) loops were performed. Inspiratory capacity (IC) of each animal was determined by the mean of the last two recruitment maneuvers, and quasi-static compliance (Cst) as a measure of lung distensibility was determined by the mean of the three pressure controlled, quasi-static PV loop values.

Administration of recombinant Flt3L in mice

Flt3L KO mice received daily subcutaneous (s.c.) injections of either vehicle (PBS supplemented with 0.1 % human serum albumin; Baxalta, Bannockburn, Illinois) or recombinant Flt3L (rFtl3L, 10 µg per mouse) for nine consecutive days, as previously described (9). To assess the therapeutic effect of rFlt3L on AdTGF-β1 induced pulmonary fibrosis in WT mice, animals were treated with vehicle or 15 µg rFlt3L s.c. for 10 consecutive days.

RNA sequencing analysis of CD11b^{pos} DC from mice with established pulmonary fibrosis

CD11b^{pos} DC were purified from the lungs of control vector or AdTGF-β1 exposed WT mice (day 14 post-treatment) by high-speed cell sorting. DNA-digested RNA samples were quantified and purity was determined with the Nanodrop ND-1000 spectrophotometer (Peqlab). RNA integrity was confirmed with an Agilent

Tort Tarrés M, *et al. Thorax* 2019; 0:947–957. doi: 10.1136/thoraxjnl-2018-212603

Bioanalyzer 2100 using either RNA 6000-Nano or -Pico assay (Agilent Technologies). Subsequently, samples were subjected to RNA sequencing analysis as described below. RNA-sequencing reads were aligned with Star (10), and read counts were extracted using HTSeq (11). Differential expression analysis was performed with DESeq2 (12). P-values were adjusted with Benjamini-Hochberg FDR (13). Over-representation analysis for specific gene sets was assessed with odds ratios and the Fisher Exact Test.

RNA sequencing and raw data processing

One ng of total RNA was used for library preparation with the 'SMARTer Stranded Total RNA-Seq Kit–Pico Input Mammalian' (Takara/Clontech) according to the manufacturer's recommendations. Generated libraries were barcoded by dual indexing approach and were finally amplified by 14 cycles of PCR. Fragment length distribution of generated libraries was monitored using Bioanalyzer High Sensitivity DNA Assay (Agilent Technologies). Quantification of libraries was performed by use of the Qubit® dsDNA HS Assay Kit (ThermoFisher Scientific). For sequencing, equal molar amounts of twelve libraries in total were pooled, denatured with NaOH and finally diluted to 1.5 pM according to the Denature and Dilute Libraries Guide (Document # 15048776 v02; Illumina). 1.3 ml of denatured pool were loaded on an Illumina NextSeq 550 sequencer using a High Output Flowcell for 75 bp single reads (#FC-404-2005; Illumina). For raw data processing and quality control, BCL files were converted to FASTQ files using bcl2fastq Conversion Software version 2.16.0.10 (Illumina). The FASTQ files were adapter and quality trimmed using Trim Galore! (version 0.4.1) with default settings as described in the User Guide except for the setting of the quality cutoff (-q/--quality) which was set to a Phred score of 15. Trim Galore! used Cutadapt (version 1.9.1) as subroutine. Quality control of FASTQ files

Tort Tarrés M, *et al. Thorax* 2019; 0:947–957. doi: 10.1136/thoraxjnl-2018-212603

was performed by FastQC (version 0.11.4) before and after trimming. After trimming, FASTQ files were mapped against a reference genome with the splice-aware aligner STAR (version 2.5.0c) to generate BAM files. BAM files were built in a 2-pass Mapping (--twopassMode Basic) and were finally sorted (--outSAMtype BAM SortedByCoordinate). All other settings were left as described in the manual. The genome index files were created by STAR with default settings using Mus musculus sequence and annotation data (UCSC, build mm9) available on illumina's iGenome site (http://support.illumina.com/sequencing/sequencing_software/igenome.html). The average number of reads entering the mapping process across all analyzed samples was 33.7 million. The average percentage of uniquely mapped reads was 78.2 %, of reads mapped to multiple loci was 11.8 %, and of unmapped reads was 9.6 %. Transcriptomic data have been deposited at the Gene Expression Omnibus (GEO) data repository (accession number GSE116210).

Real-time RT-PCR

Analysis of gene expression of MMP-2, MMP-14 and TIMP-2 in sorted lung CD11b^{pos} and CD103^{pos} DC subsets was done using real-time RT-PCR as reported recently (6). PCR primers were designed by Primer Express software (Applied Biosystems, Warrington, UK) according to gene sequence data from GenBank: MMP-2 (NM_008610.2), MMP-14 (NM_008608.4), TIMP-2 (NM_011594.3) and β-actin (NM_007393.3). For normalization, β-actin was used as a housekeeping gene and mean-fold changes were calculated using the $2^{-\beta\Delta CT}$ method (34). Each sample was tested in duplicate and a no-template control was included per amplification reaction.

Statistical analysis

Statistical analysis was performed using the software GraphPad Prism Version 6. All data are given as median ± IQR. Significant differences between experimental groups were determined by Mann-Whitney U test or two-way ANOVA, as indicated. Comparisons between survival curves were analyzed by log-rank test. Statistically significant differences between groups were assumed when p-values were < 0.05.

Tort Tarrés M, *et al. Thorax* 2019; 0:947–957. doi: 10.1136/thoraxjnl-2018-212603

Supplementary figures

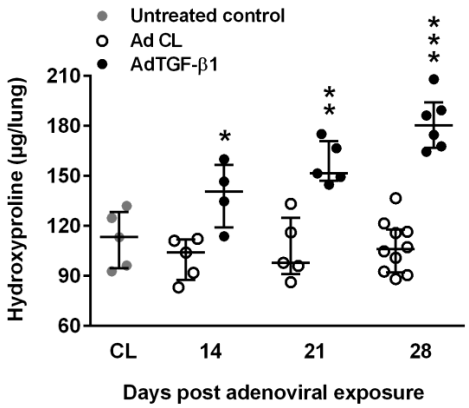

Figure S1. Collagen contents in lungs of WT mice exposed to AdTGF-β1. Quantification of hydroxyproline levels in lungs of untreated control mice (grey dots), or control vector exposed mice (white dots) or AdTGF-β1 exposed mice (black dots) at the indicated time points. Data are shown as median ± IQR of n=4-10 mice and are representative of two independent experiments. *p<0.05, **p<0.01, ***p<0.001 vs. control vector using Mann-Whitney U test.

Tort Tarrés M, *et al. Thorax* 2019; 0:947–957. doi: 10.1136/thoraxjnl-2018-212603

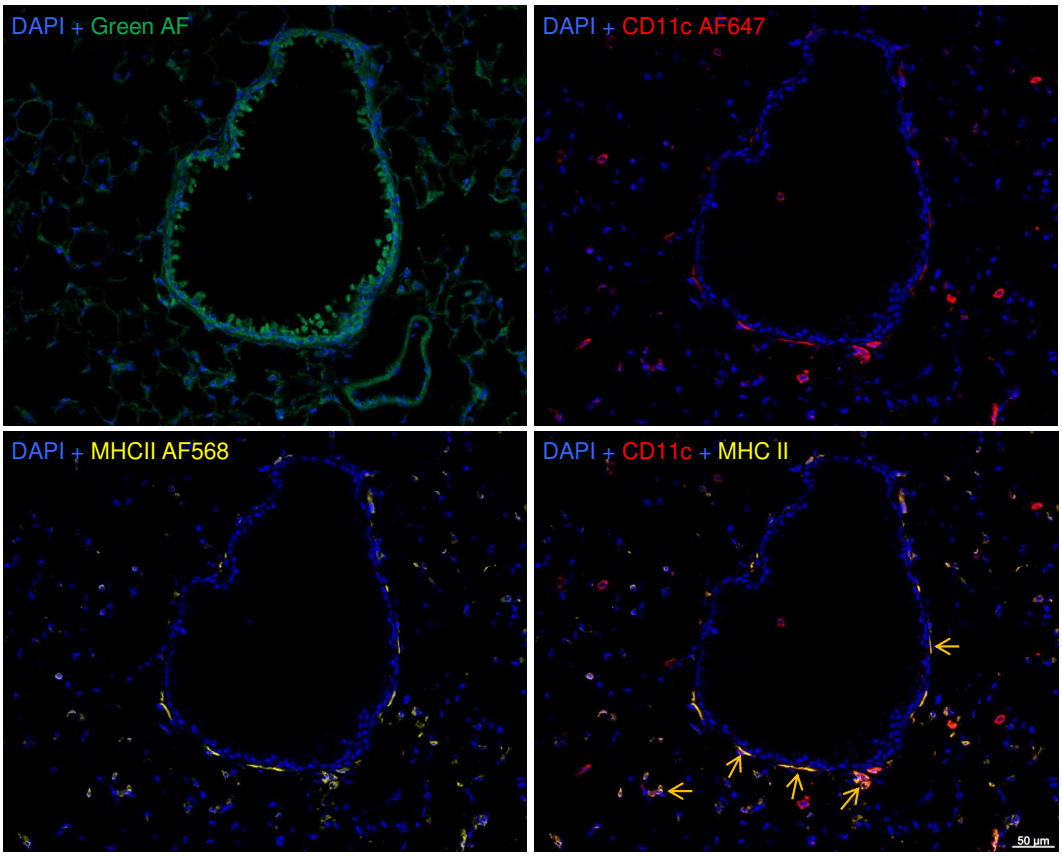

Figure S2. Immunofluorescence analysis of lung DC in control vector exposed mice. Frozen tissue sections were prepared from lungs of mice exposed to control vector (14 days, A). Lung tissue sections were stained with nuclear DAPI stain and purified rat anti-mouse MHCII, followed by goat anti-rat-AF568, and were then washed and subsequently stained with AF647-conjugated rat anti-mouse CD11c antibodies. Lung green autofluorescence (green AF) was used for topographical purposes (see quadrant 1 DAPI + green AF). Quadrant 4 illustrates the overlay of panels 2 (DAPI + Cd11c-AF647) and 3 (DAPI + MHCII-AF68). Orange arrows depict lung DC within alveolar septae and the bronchial compartment. Fluorescence images are representative of four independent analyses. Original magnification, x 20.

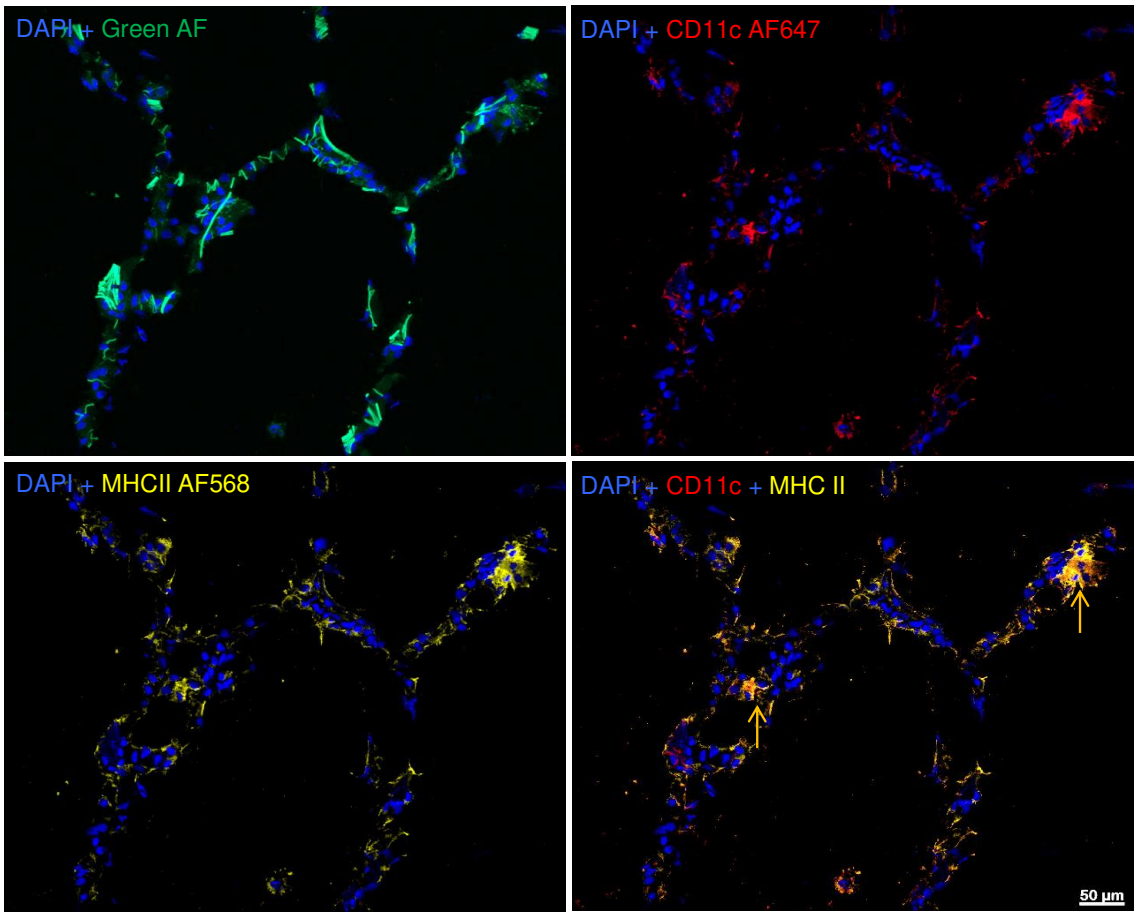

Figure S3. Immunofluorescence analysis of lung DC in human lung tissue specimen from disease control patients. Frozen lung tissue sections were stained with nuclear DAPI stain and purified mouse anti-human MHCII antibody, followed by incubation with AF568-conjugated goat anti-mouse secondary antibody, and were then washed and stained with AF647-conjugated anti-human CD11c antibody. Green autofluorescence (AF) of lung tissue was exploited for topographical purposes (quadrant 1, DAPI + green AF). Quadrant 4 illustrates the overlay of panels 2 (DAPI + CD11c-AF647) and 3 (DAPI + MHCII-AF68). Orange arrows indicate lung DC within alveolar septae. Fluorescence images are representative of two independent determinations. Original magnification, x 40. Bar graph, 50 µm.

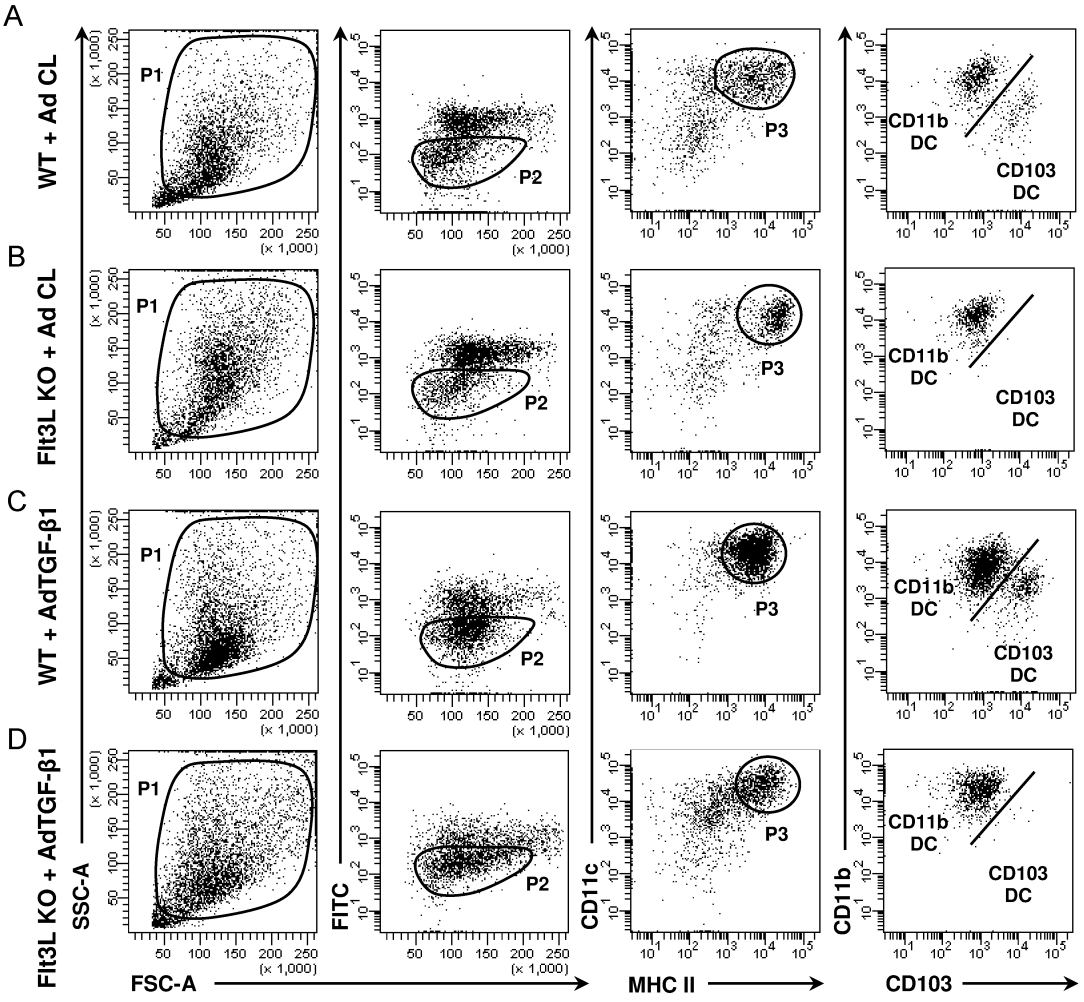

Figure S4. FACS gating strategy for identification of CD11b^{pos} and CD103^{pos} DC in lung tissue of WT and Flt3L KO mice exposed to control vector or AdTGF-β1. (A-D) FACS gating of CD11b^{pos} and CD103^{pos} DC subsets in (A,C) WT mice and (B,D) Flt3L KO mice 14 days post control vector (Ad CL) or AdTGF-β1 exposure. Classical DC subsets were gated according to their forward scatter area (FSC-A) versus side scatter area (SSC-A) characteristics and their low green autofluorescence properties, in conjunction with their CD11c^{pos}, MHCII^{pos}, CD11b^{hi}, CD103^{neg} (CD11b^{pos} DC) or CD11c^{pos}, MHCII^{pos}, CD11b^{low}, and CD103^{pos} (CD103^{pos} DC) antigen expression profiles.

Tort Tarrés M, *et al. Thorax* 2019; 0:947–957. doi: 10.1136/thoraxjnl-2018-212603

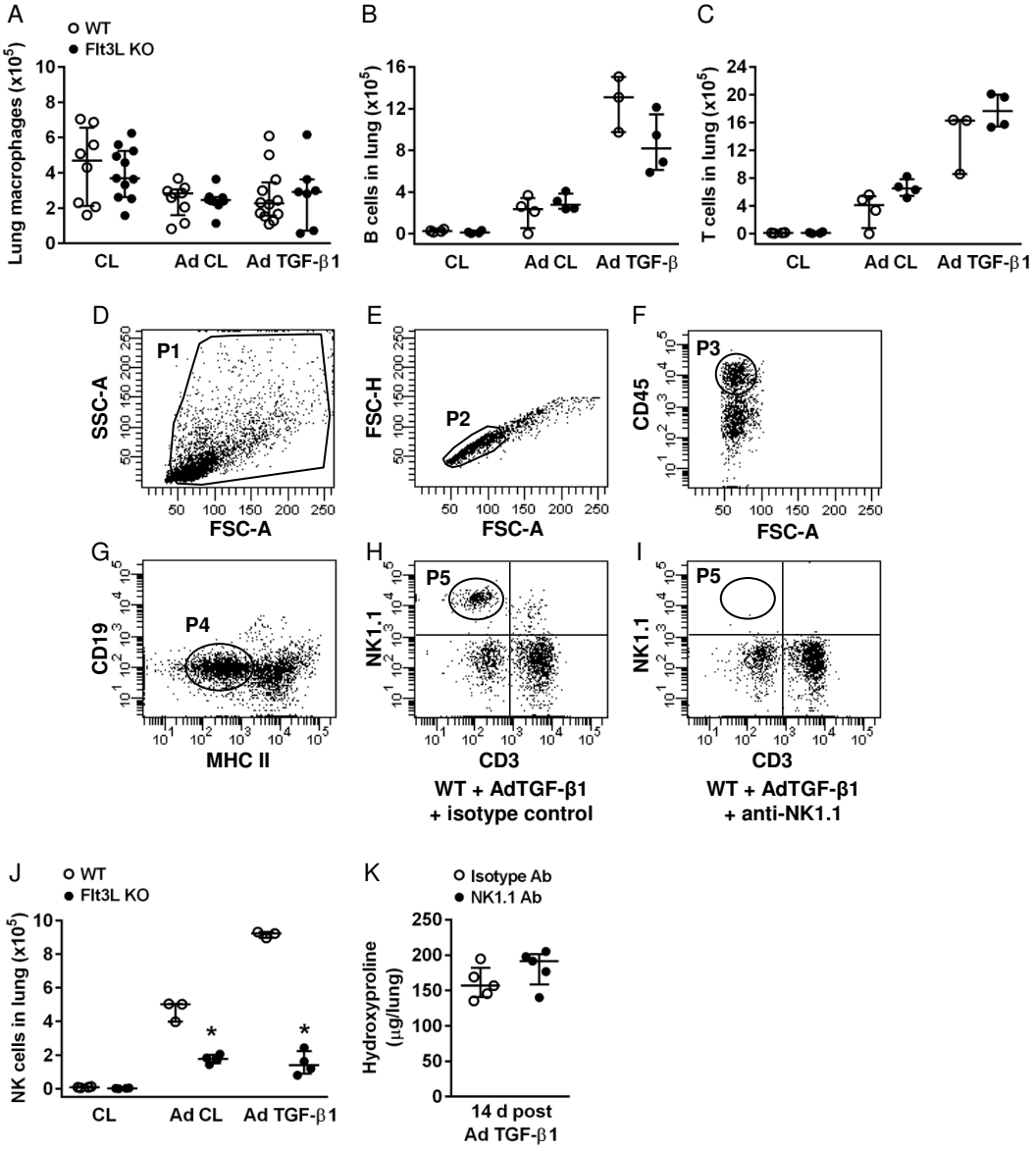

Figure S5. Effect of NK cell depletion on AdTGF-β1 induced lung fibrosis in WT mice. (A-C) WT and Flt3L KO mice were either left untreated (CL), or were exposed to control vector or AdTGF-β1, and alveolar macrophages (A), B cells (B), and T cells (C) were quantified in lung tissue at day 14 post-treatment. (D-I) Gating strategy for FACS-based identification of NK cells in lung tissue of WT mice exposed to AdTGF-β1 for 14 days. After gating according to FSC-A/ SSC-A (P1 in D) and FSC-A/FSC-H (P2 in E), the fraction of $CD45^{pos}$ (P3 in F), and $CD19^{neg}$, $MHCII^{neg}$ leukocytes was

sub-gated (P4 in G), followed by identification of NK cells as $CD3^{neg}$, $NK1.1^{pos}$ lymphoid cells (P5 in H), which were depleted after administration of anti-NK1.1 Ab (P5 in I). (J) Quantification of NK cells in untreated (CL), or Ad CL or AdTGF-β1 exposed WT and Flt3L KO mice at day 14 post-treatment. (K) Hydroxyproline contents in the lungs of NK cell-depleted (black dots) versus non-depleted (isotype Ab, white dots) WT mice exposed to AdTGF-β1 for 14 days. Data are shown as median ± IQR of n=7-12 (A), n=3-4 (B,C,J), or n=5 (K) mice and are representative of two independent experiments. *$p<0.05$ vs. respective treatment in WT mice using Mann-Whitney U test.

Tort Tarrés M, *et al. Thorax* 2019; 0:947–957. doi: 10.1136/thoraxjnl-2018-212603

A

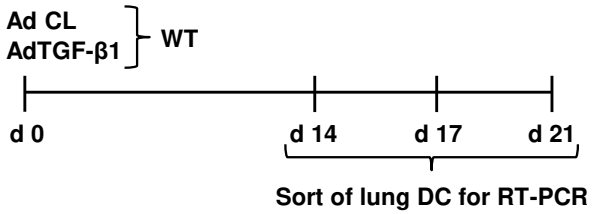

B

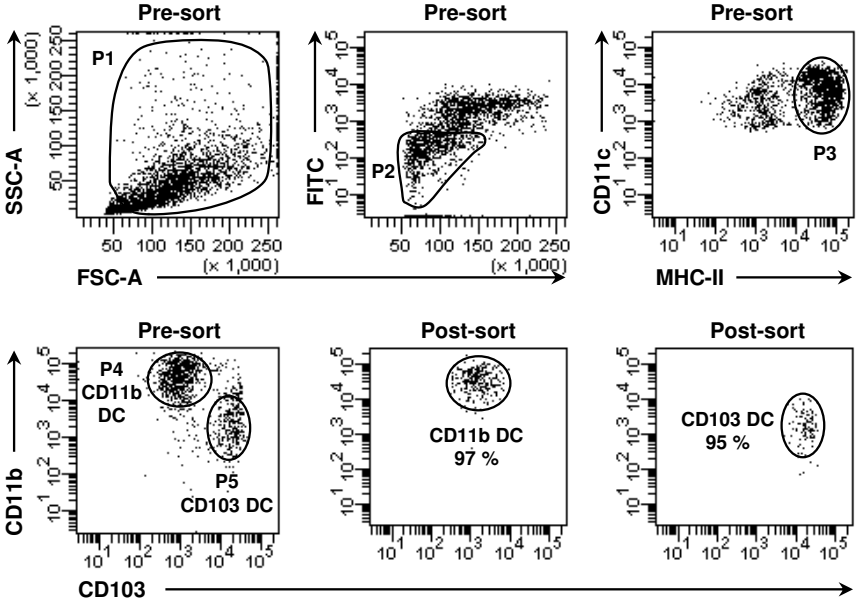

Figure S6. Flow-sort of lung DC subsets of WT mice exposed to control vector or AdTGF-β1. (A) WT mice were exposed to control vector (Ad CL) or AdTGF-β1 and were subjected to CD11b^{pos} DC and CD103^{pos} DC sort for subsequent RT-PCR of fibrosis-related markers. (B) Gating of DC subsets according to their forward scatter area (FSC-A) versus side scatter area (SSC-A) characteristics (P1) and their low green autofluorescence properties (P2), in conjunction with their CD11c^{pos}, MHCII^{pos} (P3), CD11b^{hi}, CD103^{neg} (CD11b^{pos} DC) or CD11c^{pos}, MHCII^{pos}, CD11b^{low}, and CD103^{pos} (CD103^{pos} DC) antigen expression profiles. CD11b^{pos} DC and CD103^{pos} DC post-sort purities were > 95 %.

Tort Tarrés M, *et al. Thorax* 2019; 0:947–957. doi: 10.1136/thoraxjnl-2018-212603

References

1. McKenna HJ, Stocking KL, Miller RE, Brasel K, De Smedt T, Maraskovsky E, Maliszewski CR, Lynch DH, Smith J, Pulendran B, et al. Mice lacking flt3 ligand have deficient hematopoiesis affecting hematopoietic progenitor cells, dendritic cells, and natural killer cells. *Blood* 2000;95(11):3489-3497.

2. Meredith MM, Liu K, Darrasse-Jeze G, Kamphorst AO, Schreiber HA, Guermonprez P, Idoyaga J, Cheong C, Yao KH, Niec RE, et al. Expression of the zinc finger transcription factor zdc (zbtb46, btbd4) defines the classical dendritic cell lineage. *The Journal of experimental medicine* 2012;209(6):1153-1165.

3. Sime PJ, Xing Z, Graham FL, Csaky KG, Gauldie J. Adenovector-mediated gene transfer of active transforming growth factor-beta1 induces prolonged severe fibrosis in rat lung. *J Clin Invest* 1997;100(4):768-776.

4. Knippenberg S, Ueberberg B, Maus R, Bohling J, Ding N, Tort Tarres M, Hoymann HG, Jonigk D, Izykowski N, Paton JC, et al. Streptococcus pneumoniae triggers progression of pulmonary fibrosis through pneumolysin. *Thorax* 2015;70(7):636-646.

5. Steinwede K, Henken S, Bohling J, Maus R, Ueberberg B, Brumshagen C, Brincks EL, Griffith TS, Welte T, Maus UA. Tnf-related apoptosis-inducing ligand (trail) exerts therapeutic efficacy for the treatment of pneumococcal pneumonia in mice. *The Journal of experimental medicine* 2012;209(11):1937-1952.

6. Behler-Janbeck F, Takano T, Maus R, Stolper J, Jonigk D, Tort Tarres M, Fuehner T, Prasse A, Welte T, Timmer MS, et al. C-type lectin mincle recognizes glucosyl-diacylglycerol of streptococcus pneumoniae and plays a protective role in pneumococcal pneumonia. *PLoS pathogens* 2016;12(12):e1006038.

7. Lopez-Rodriguez E, Boden C, Echaide M, Perez-Gil J, Kolb M, Gauldie J, Maus UA, Ochs M, Knudsen L. Surfactant dysfunction during overexpression of tgf-beta1 precedes profibrotic lung remodeling in vivo. *American journal of physiology Lung cellular and molecular physiology* 2016;310(11):L1260-1271.

8. Hantos Z, Daroczy B, Suki B, Nagy S, Fredberg JJ. Input impedance and peripheral inhomogeneity of dog lungs. *Journal of applied physiology* 1992;72(1):168-178.

9. von Wulffen W, Steinmueller M, Herold S, Marsh LM, Bulau P, Seeger W, Welte T, Lohmeyer J, Maus UA. Lung dendritic cells elicited by fms-like tyrosine 3-kinase ligand amplify the lung inflammatory response to lipopolysaccharide. *Am J Respir Crit Care Med* 2007;176(9):892-901.

10. Dobin A, Davis CA, Schlesinger F, Drenkow J, Zaleski C, Jha S, Batut P, Chaisson M, Gingeras TR. Star: Ultrafast universal rna-seq aligner. *Bioinformatics* 2013;29(1):15-21.

11. Anders S, Pyl PT, Huber W. Htseq--a python framework to work with high-throughput sequencing data. *Bioinformatics* 2015;31(2):166-169.

12. Love MI, Huber W, Anders S. Moderated estimation of fold change and dispersion for rna-seq data with deseq2. *Genome Biol* 2014;15(12):550.

13. Benjamini Y, Hochberg, Y. Controlling the false discovery rate: A practical and powerful approach to multiple testing. *Journal of the Royal Statistical Society* 1995;57(1):289-300.